Reception: **June 28, 2024** | Acceptance: **Octubre 8, 2025** | Publication: **February 1, 2026**

Synthesis of Zinc Oxide by the hydrothermal method: effect of aging time

—

Kervin Gabriel Rincón Soto[1] • kerbriel92@gmail.com
ORCID: 0009-0008-1775-4796

Edna Iris Ríos Valdovinos[1] • edna.rios@unicach.mx
ORCID: 0000-0003-2755-2385

Maricruz Jiménez Cerda[1] • jimenezmary243@gmail.com
ORCID: 0009-0001-7205-2390

José Francisco Pola Albores[1] • francisco.pola@unicach.mx
ORCID: 0000-0002-8843-5708

1 Sustainable Materials and Processes Laboratory (LaMPSus) / Institute for Research and Innovation in Renewable Energy / Universidad de Ciencias y Artes de Chiapas (UNICACH), Tuxtla Gutiérrez, Chiapas, México.

To quote this article:
Rincón Soto, K. G., Ríos Valdovinos, E. I., Jiménez Cerda, M., & Pola Albores, J. F. Síntesis de óxido de zinc mediante el método hidrotermal: efecto del tiempo de envejecimiento. *Espacio I+D, Innovación más Desarrollo, 15*(43). https://doi.org/10.31644/IMASD.43.2026.a04

— Abstract—

Nanomaterials have many applications, including in health, the environment, energy, and electronics. Their performance in these areas depends on specific optical, morphological, and physical properties, which are determined by how they are prepared. Factors such as reaction temperature, solution pH, precursor concentration, type of solvent, stirring rate, and aging time are currently studied. The objective of this work is to study the effect of aging time on particle formation at different durations: 24 h, 12 h, and without aging, at two pH values, 7 and 9. The synthesis was done using the hydrothermal method, with zinc chloride ($ZnCl_2$) and ammonium hydroxide (NH_4OH) as precursors. The samples were characterized by X-ray Diffraction (XRD), Scanning Electron Microscopy (SEM), and Ultraviolet-Visible Spectroscopy (UV-Vis). At pH 7, the samples mainly formed ZnO, with stronger and sharper peaks after 24 hours of aging. At pH 9, aging promoted the formation of the simonkolleite phase. In both cases, particle size increased with aging time, reaching about 40 nm for pH 7 and 36 nm for pH 9. The band gaps were 3.20 eV for ZnO and 3.24 eV for simonkolleite. It was found that pH plays an important role in phase formation and, together with aging time, affects the morphology of the materials.

Keywords:

ZnO, simonkolleite, nanoparticles, hydrothermal method.

Nanotechnology is one of the research fields that has gained the most attention in recent years, as the development of new materials at nanometric scales <100 nm promotes emerging technology in the transition toward more environmentally friendly energy models. Nanomaterials display physical and chemical properties different from macroscopic-sized materials, primarily because they possess greater specific surface area per unit volume (Echeverri et al., 2021). The interest in nanomaterial development is highlighted due to its substantial growth; enhanced understanding of the relationship between properties and structures is anticipated, along with progress in manufacturing techniques facilitating their applications across various fields, including medicine, optics, electronics, textiles, cosmetics, catalysis, and energy (Malaret et al., 2023).

ZnO nanoparticles are distinguished by their stable structure; their non-toxic nature features a wide bandgap of 3.37 eV and exciton binding energy of 60 meV (Widiyandari et al., 2023). Maintaining competitiveness with other materials requires improving synthesis methods for high-quality, low-cost production (Guzmán et al., 2022). This metal oxide is produced via diverse physical and chemical methods. Amongdifferent synthesis routes, the hydrothermal approach is particularly notable for being eco-friendly, economical, straightforward, and easily controllable. Additionally, nanoparticles obtained by this method demonstrate high crystallinity relative to those produced through other solution-based processes (Sansenya et al., 2021).

Studies such as that of Pittayathorn et al. (2023), which examined the beneficial impact of ZnO aging, attributed this to increased oxygen vacancy formation in the material. These findings highlight the importance of investigating factors including aging and pH modification in ZnO and simonkolleite formation, motivating this study focused on understanding their effects on crystal structure, morphology, and other relevant material properties. Adjusting synthesis parameters in these methods enables tailoring material properties to specific industrial application requirements, ensuring reproducibility, efficiency, and scalability (Guzmán et al., 2022).

MATERIALS AND METHODS

Synthesis employed the hydrothermal method. A 0.1 mol/L ZnCl2 solution in 0.1 L H 2O was prepared and continuously stirred on a thermomagnetic stirrer (Thermo Scientific) for 30 min at room temperature. The pH was adjusted to 7 and 9 by slowly adding 1 mol/L NH 4OH dropwise. The mixture underwent three aging conditions: 24, 12, and 0 h, with the latter serving as an unaged control. All treatments were conducted in darkness at room temperature. Each solution was then transferred to a stainless-steel autoclave reactor (17.48x5x5 cm) and heated to 200 °C for 180 min in a convection oven (Binder model). The mixture underwent gravity filtration, and the remaining solution was centrifuged at 3500 rpm (≈1500g) for 15 min using a centrifuge (MPW 223e). The precipitate was washed twice with

water and methanol, dried on a thermomagnetic stirrer (Thermo Scientific), and ultimately calcined at 400 °C for 240 min in a muffle furnace (Felisa-341).

Characterization

Sample crystal structure was determined via X-Ray Diffraction (XRD) on a Rigaku Ultima IV diffractometer, utilizing Cu Kα radiation with λ=1.5418×10−10 or 1.5418 Å, 2θ/θ scan angle, scan speed of 2°per minute, and scan range of 20° to 80°. Operating conditions included 40 kV voltage, 44 mA current, and Bragg-Brentano geometry. Morphology was examined by Scanning Electron Microscopy (SEM) using Hitachi FE-SEM S-5500 equipment at various magnifications. Diffuse reflectance spectroscopy (DRS) was performed on a Shimadzu UV-Vis-NIR-3600 spectrophotometer equipped with an integrating sphere across the 200 to 800 nm range.

Crystal size was determined by the Scherrer equation corresponding to equation (1).

$$L = \frac{k\lambda}{FWHM \cos\theta} \qquad \text{(Equation 1)}$$

Where: $\boldsymbol{k}$ represents the Scherrer constant valued at 0.89, λ denotes Cu Kα radiation wavelength, FWHM (Full Width at Half Maximum) indicates the (hkl) peak half-width, and θ designates the angular position of XRD peaks, half of 2θ.

Bandgap (*Eg*) calculations employed two formulas: the Kubelka-Munk equation, equation (2), and the Tauc equation, equation (3).

$$R = \frac{(1-R)^2}{2R} \qquad \text{(Equation 2)}$$

$$\alpha h\nu = A\left(h\nu - E_g\right)^n \qquad \text{(Equation 3)}$$

Where R represents the experimentally measured diffuse reflectance, α denotes the material's absorption coefficient, hv indicates the indicent photon energy (eV), A is a proportionality constant, and "n" corresponds to the electronic transition exponent-in this case $^1/_2$ according to Hedge et al. (2024) attributed to the direct transition nature in ZnO and crystalline Simonkolleite solid ($Zn_5(OH)_8Cl_2 \cdot H_2O$).

RESULTS AND DISCUSSION

X-Ray Diffraction (XRD)

Previously synthesized samples underwent XRD characterization. Figure 1 displays diffractograms at various aging times and pH levels. Analysis employed PDXL version 1.8 software. Figure 1a revealed 11 diffraction signals at angles of 32°, 34°, 36°, 47°, 56°, 62°, 66°, 67°, 68°, 72°, and 76°. These values match the data from PDF card 01-074-9943 at a 2θ angle, indicating the formation of ZnO without impurities

and with a hexagonal wurtzite-type structure in Zincite phase, consistent with that reported by Sofianos et al. (2021). This suggests that moderate OH^- concentration at pH 7 facilitates zinc hydroxide $Zn(OH)_2$ formation. This behavior is attributable to achieving suitable chemical equilibrium at neutral pH for$Zn(OH)_2$ functioning as intermediate precursor (Yabalak et al., 2024). During hydrothermal processing, this compound undergoes dehydration, directly yielding wurtzite structure-the thermodynamically most stable phase under these conditions (Cardoso et al., 2022).

The formation of ZnO requires a series of reactions depending on the pH of the solution, as indicated below.

$$ZnCl_2 + H_2O \rightarrow Zn^{2+} + 2Cl^- + H_2O \quad \text{(Equation 4)}$$

$$NH_4OH \rightarrow NH_4^+ + OH^- \quad \text{(Equation 5)}$$

$$Zn^{2+} + 2OH^- \rightarrow Zn(OH)_2 \quad \text{(Equation 6)}$$

$$Zn(OH)_2 \rightarrow ZnO + H_2O \quad \text{(Equation 7)}$$

As reported by Herrera et al. (2010), equation (4) depicts the initial synthesis process where $ZnCl_2$ dissociates in water, yielding Zn_2^+(zinc ion) + $2Cl^-$ (chloride ion). Equation (5) shows NH_4OH releasing NH_4^+ (ammonium ion) and OH^- (hydroxyl ion). The presence of OH^- ein the reaction is important, as the formation of $Zn(OH)_2$ depends on it (6), which slowly forms ZnO and water (7). The XRD results in Figure 1a suggest that the longer the solution was aged, the more complete the conversion of $Zn(OH)_2$ a ZnO. Este efecto se vio favorecido en todas las muestras a pH 7, principalmente en la muestra con 24 h de envejecimiento, seguida de las de 12 y 0 h. A 24 h, los picos del difractograma son más definidos e intensos que los de 12 y sin envejecer. Esto se asocia a que tras el envejecimiento, la conversión de $Zn(OH)_2$ to ZnO is greater, and there is a higher predisposition prior to the heat treatment. Furthermore, the hydrothermal process temperature of 400 °C facilitates crystallization, improving ZnO formation. The crystal size was calculated using equation (1) with the (101) plane, yielding 36 nm for 24 h, and 29 nm for both 12 and 0 h, attributed to the aging effect. The increasing in crystal size, calculated using the Scherrer equation, with aging time can be attributed to structural maturation phenomena that occur during the resting of the precursor solution. Primarily, the Ostwald ripening process (Sarkar et al., 2023) promotes the re-dissolution of smaller particles, which are thermodynamically less stable due to their high surface energy, and the subsequent redeposition of material onto larger particles, favoring crystal growth. In parallel, the primary nanoparticles of $Zn(OH)_2$ (ZnO precursor) or Simonkolleite precursors have time to reorient, coalesce, and sinter in solution (Hernández-Díaz et al., 2024), reducing internal defects and grain boundaries, which

results in larger individual crystallites with improved crystallinity, as evidence by the intensification and narrowing of the XRD peaks.

On the other hand, in Figure 1b the diffraction signals were observed at angles of 22°, 24°, 28°, 30°, 31°, 32°, 33°, 36°, 44°, and 56° at a 2θ angle, indexed with PDF card 00-0007-0155 corresponding to Simonkolleite with a trigonal structure, space group R-3m(166) and unit cell of a= 6.3400Å, b=6.3400 Å, c=23.6600Å, α= 90.000°, β=90.000°, γ=120.000°, coinciding with the same crystallographic card reported by He et al., (2019). The high concentration of ion at pH 9 leads to a different synthesis route, resulting in the formation of $Zn_5(OH)_8Cl_2 \cdot H_2O$. In this material, Cl^- ions are an integral part of the structure, incorporated between the zinc and hydroxide layers that characterize its crystal lattice, as shown in the following chemical reactions.

$$ZnCl_2 + H_2O \rightarrow Zn^{2+} + 2Cl^- + H_2O \qquad \text{(Ecuación 8)}$$

$$NH_4OH \rightarrow NH_4^+ + OH^- \qquad \text{(Ecuación 9)}$$

$$Zn^{2+} + 2OH^- \rightarrow Zn(OH)_2 \qquad \text{(Ecuación 10)}$$

$$Zn_5(OH)_2 + 2Cl^- + H_2O \rightarrow Zn_5(OH)_8Cl_2 \cdot H_2O \qquad \text{(Ecuación 11)}$$

The synthesis process follows reactions (4), (5), and (6), but under pH 9 conditions, the high concentration of OH^- and Cl^- shifts the equilibrium toward reaction (11), where five units of $Zn(OH)_2$ combine with two Cl^- ions and one water molecule to directly form the $Zn_5(OH)_8Cl_2 \cdot H_2O$ structure. This can be confirmed in Figure 1b, in which the 24 h sample is observed to present the most intense and well-defined diffraction peaks for Simonkolleite, indicating the highest degree of crystallinity. Unlike the aged sample, the 12 h sample exhibits lower intensity peaks, while the unaged sample presents the weakest and broadest peaks, suggesting an incomplete transformation of the precursor (He et al., 2019). As observed at pH 7, the heat treatment at 400 °C for 3 h played a significant role in the formation and crystallization of all three samples, particularly in the structural reorganization leading to the formation of Simonkolleite from the available ions (Qu et al., 2023). The crystallite size was determined using the Scherrer equation (1), yielding 31 nm for the 24 h sample, 24 nm for the 12 h sample, and 24.86 nm for the unaged sample.

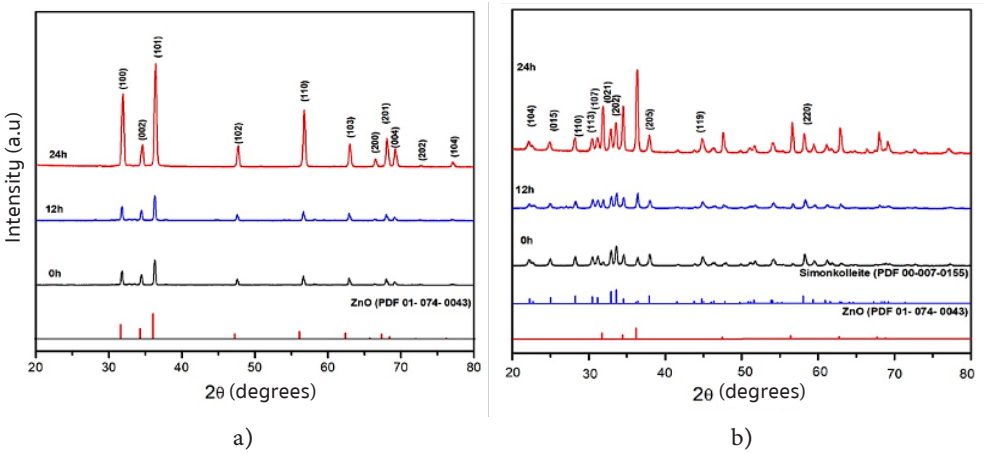

Figure 1. X-ray diffractograms: a) ZnO with a hexagonal wurtzite-type structure is confirmed following heat treatment at 200 °C and calcination at 400 °C and pH 7; b) the formation of Simonkolleite was favored under the same synthesis conditions by adjusting the pH to 9

Scanning Electron Microscopy (SEM)

The SEM micrographs are presented in Figure 2 at a magnification of 2000 X. Figure 2a shows platelet-shaped agglomerates with irregular morphology (Soto et al., 2023). These agglomerates display a variable size distribution, suggesting that primary particles have bonded together to form larger particles. This is attributed to the fact that during synthesis, $Zn(OH)_2$ initiates the nucleation process through aging, giving rise to small primary particles (Sarkar et al., 2023). The growth of these particles occurs through the adsorption of additional Zn^{2+} and OH^- ions from the solution. Hernández-Díaz et al. (2024), demonstrated that primary ZnO particles tend to agglomerate due to electrostatic interactions and Van de Waals forces. This agglomeration process can give rise to the formation or larger and more complex structures, such as slabs or platelets. These platelets form when secondary particles (which, as reported by Hernandez- Díaz et al. (2024), are aggregates of primary particles) grow preferentially along certain crystallographic directions. During aging, the solution is kept undisturbed, allowing chemical reactions as well as nucleation and growth processes to proceed. Longer aging times promote greater agglomeration, resulting in more defined and larger structures.

Figure 2b, corresponding to the 24 h sample at pH 9, also shows platelet agglomerates with irregular morphologies, attributed to the high concentration of OH^- and Cl^- ions that promote their formation (Shaoqing et al., 2023). The abundance of OH^- ions has facilitated the formation of Simonkolleite, whose compact and well-defined structure is evident in the SEM micrographs.

The formation of these irregular platelets indicates that the alkaline environment and the extended aging period have allowed particles to nucleate and grow preferentially along specific crystallographic directions. This result underscores the importance of pH and aging time on the final morphology of

materials synthesized by hydrothermal methods, highlighting how these factors can influence the structure and properties of the resulting nanomaterials.

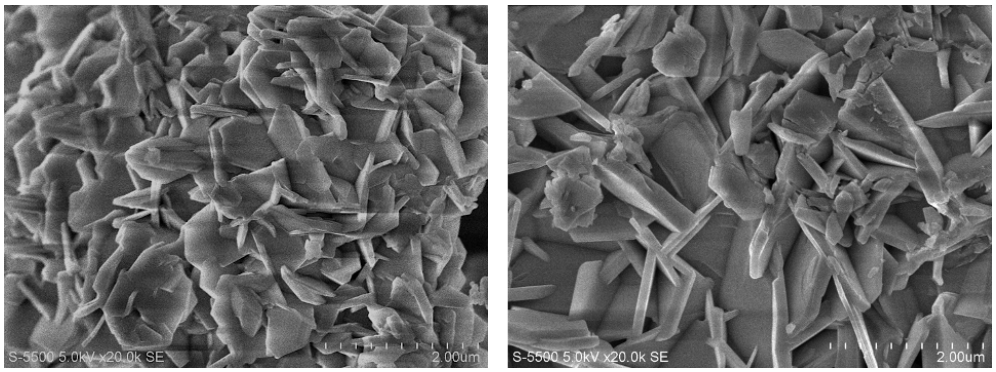

a) b)

Figure 2. Scanning Electron Microscopy at 2000 X magnification: a) 24 h at pH 7 and b) 24 h at pH 9

Diffuse Reflectance Spectroscopy (DRS)

Diffuse reflectance spectroscopy (DRS) in the UV-Vis range was employed to investigate the light absorption behavior of the samples. The obtained results are presented in Figure 3. Figure 3a shows a reflectance drop in ZnO at a wavelength of 380 nm, indicating a transition in the material's ability to absorb light in that region of the electromagnetic spectrum. Wu et al. (2019) report that this wavelength falls within the ultraviolet region, where ZnO exhibits a drop at 388 nm. All analyzed samples exhibited this same trend, confirming that pure ZnO was obtained regardless of the aging time. However, the 24 h sample shows a slight increase in reflectance, despite the drop occurring at the same wavelength across all samples. This can be attributed to two factors: first, the larger particle size; and second, a more ordered crystalline structure, as crystal orientation can influence reflectance (Wu et al., 2019).

Figure 4 presents the bandgap energy calculation using the reflectance spectra and the Kubelka-Munk equations (2) and (3). The obtained results are shown in Figure 5. For the unaged sample, the bandgap energy is 3.22 eV, for the 12 h sample it is 3.17 eV, and for the 24 h sample it is 3.20 eV. These results agree with the bandgap values for ZnO reported in the literature (Soto, 2023).

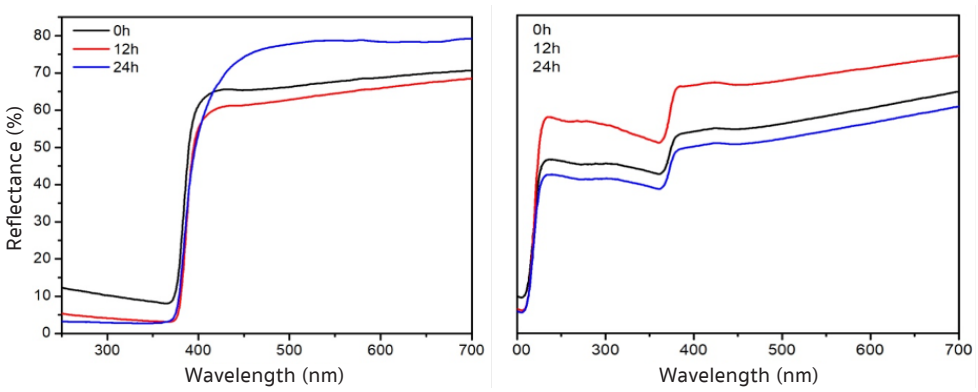

Figure 3. Diffuse reflectance spectra: a) ZnO at pH 7 with 0 h, 12 h, and 24 h, and b) ZnO at pH o with 0 h, 12h and 24 h

The UV-Vis diffuse reflectance results for Simonkolleite presented in Figure 3b, show a drop at 378 nm, followed by another in the region near 200 nm. This result is consistent with what has been reported in the literature, indicating a specific interaction of the material with UV energy (Galindo Guzmán et al., 2023). Equations (2) and (3) were once again employed for the bandgap energy calculations. The results reveal bandgap values of 3.27 eV for the o h sample, 3.17 eV for the 12 h sample, and 3.24 eV for the 24 h sample. The reflectance results in Figure 3b show no significant variations in the formation of Simonkolleite, except that the sample with the highest reflectance is the 12 h aged sample, diverging from the trend observed in the ZnO results. This variation in bandgap energy values could be attributed to the presence of defects in the crystalline lattice of the material, such as vacancies or impurities, which locally modify the electronic structure (Wu et al., 2019). Furthermore, the sample in Figure 4e presents a lower bandgap of 3.17 eV, suggesting that less energy is required for electron excitation, which could contribute to an enhanced UV energy response and, consequently, to greater light absorption compared to other aging conditions.

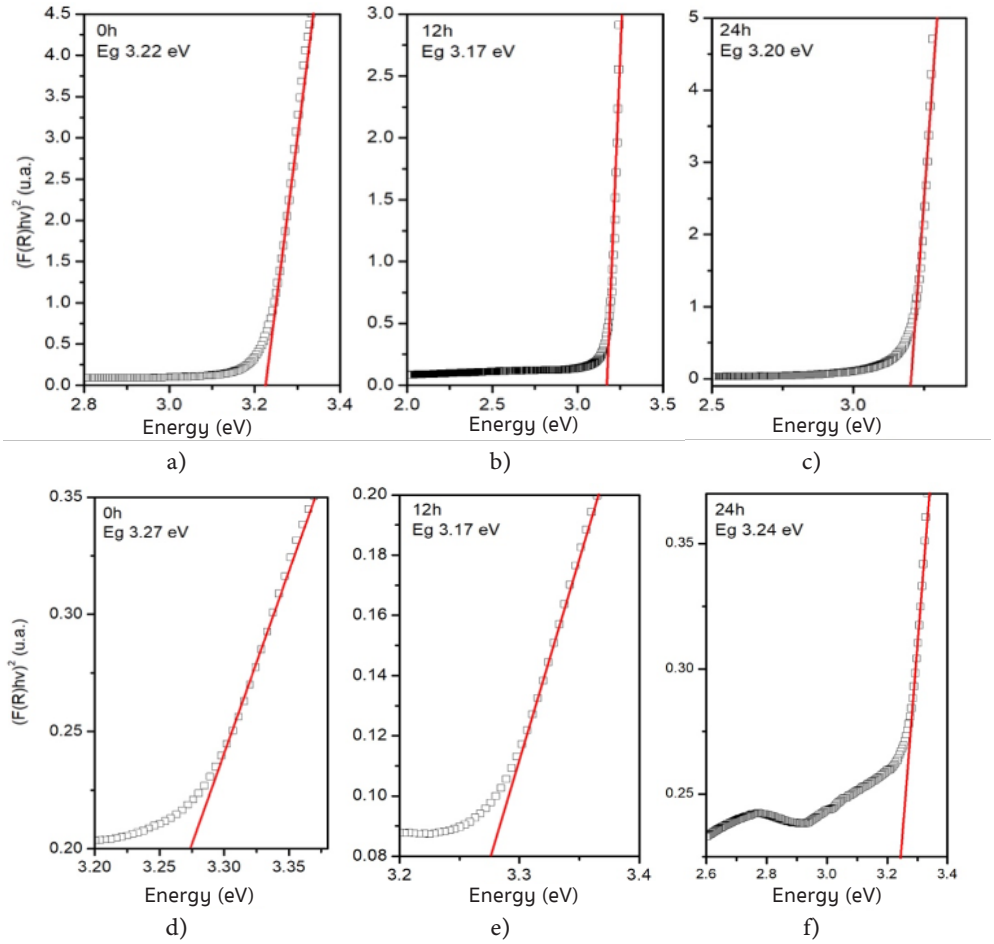

Figure 4. Bandgap of nanomaterials: pure ZnO at a) 0 h, b) 12 h, c) 24 h, and Simonkolleite at d) 0 h, e) 12 h, and f) 24 h.

CONCLUSIONS

Based on the results obtained, ZnO and Simonkolleite were successfully synthesized via the hydrothermal method using $ZnCl_2$ and NH_4OH as precursors. It is therefore concluded that pH and aging time are key parameters in the hydrothermal synthesis of nanomaterials, as they govern the formation and evolution of the crystalline phases.

The results indicate that pH directly influences phase formation: at pH 7, ZnO is obtained through thermal dehydration of $Zn(OH)_2$, whereas at pH 9, the excess of OH^- and Cl^- ions promotes the formation of Simonkolleite. Aging time affects the nucleation and development of the material, as the unaged sample 0 h exhibited the lowest values of crystallite size and crystallinity, while a period of 24 h produced as significant increase in both parameters for the two phases.

The bandgap values of 3.20 eV for ZnO and 3.24 eV for Simonkolleite confirmed that aging primarily modifies the structural parameters without altering the fundamental electronic transitions. These findings demonstrate the interplay between pH and aging time in determining the structural characteristics of nanoparticles obtained by hydrothermal methods.

REFERENCES

Cardoso, D., Narcy, A., Durosoy, S., & Chevalier, Y. (2022). The pH dependence of dissolution kinetics of zinc oxide. *Colloids And Surfaces A Physicochemical And Engineering Aspects, 650*, 129653. https://doi.org/10.1016/j.colsurfa.2022.129653

Cerda, M. J. (noviembre de 2022). *Síntesis y caracterización de ZnO para aplicaciones fotocatalíticas*. Tesis. Universidad de Ciencias y Artes de Chiapas. México.

Hernández-Díaz, Maleni N., Torres-Valencia, Nina, Miranda-Arámbula, Mariana, Ríos-Cortés, Ada M., Fernández-Luqueño, Fabián, López-Gayou, Valentín, & López-Valdez, Fernando. (2024). El rol de las plantas silvestres o cultivables de México en la síntesis de nanopartículas. *Mundo nano. Revista interdisciplinaria en nanociencias y nanotecnología, 17*(32), e00089. Epub 01 de abril de 2024.https://doi.org/10.22201/ceiich.24485691e.2024.32.69743

Galindo-Guzmán, Alma Patricia, Fortis-Hernández, Manuel, De La Rosa-Reta, Claudia Verónica, Zermeño-González, Héctor, & Galindo-Guzmán, Magdalena. (2022). Síntesis química de nanopartículas de óxido de zinc y su evaluación en plántulas de Lactuca sativa. *Revista mexicana de ciencias agrícolas, 13*(spe28), 299-308. 13 de enero de 2023.https://doi.org/10.29312/remexca.v13i28.3284

Galindo-Guzmán, Alma Patricia, Fortis-Hernández, Manuel, De La Rosa-Reta, Claudia Verónica, Zermeño-González, Héctor, & Galindo-Guzmán, Magdalena. (2022). Síntesis química de nanopartículas de óxido de zinc y su evaluación en plántulas de Lactuca sativa. *Revista mexicana de ciencias agrícolas, 13*(spe28), 299-308. Epub 13 de enero de 2023.https://doi.org/10.29312/remexca.v13i28.3284

Guzmán, A. P. (2022). Síntesis química de nanopartículas de óxido de zinc y su evaluación en plántulas de Lactuca sativa. *Revista Mexicana de Ciencias Agrícolas*, 299.

He, J., Hu, J., Mo, X., Hao, Q., Fan, Z., He, G., Wang, Y., Li, W., & He, Q. (2019). Novel photocatalyst nitrogen-doped simonkolleite $Zn_5(OH)_8Cl_2 \cdot H_2O$ with vis-up-conversion photoluminescence and effective visible-light photocatalysis. *Applied Physics. A, Materials Science and Processing (print), 125*(1), p. 1-9. https://doi.org/10.1007/s00339-018-2275-0

Hegde, V. (2024). *Study on structural, morphological, elastic and electrical properties of ZnO nanoparticles for electronic device applications*. https://doi.org/10.1016/j.jsamd.2024.100733

Herrera, Elizabeth; Cadena, Francisco; Lascano Lascano (2010). Luis Estudio de la influencia del número de lavados y del tiempo de envejecimiento en la síntesis de nanopartículas de óxido de cinc por el Método de Precipitación Controlada. *Revista Politécnica*, vol. 31 https://www.redalyc.org/pdf/6887/688773658013.pdf

Kadam, V., Jagtap, C., Alshahrani, T., Lokhande, P., Al-Ahmed, A., Patole, S.P., Khan, F., & Pathan, H.M. (2023). Synthesis and characterization of ZnO nanoparticles and their application in dye-sensitized solar cells. *Journal of Materials Science: Materials in Electronics, 34*, 1-15.

Malaret, F., Qu, S., Hadjittofis, E., Hallett, J., Smith, R., & Sedransk Campbell, K. (2023). Controlling simonkolleite crystallisation via metallic Zn oxidation in a betaine hydrochloride solution. *Nanoscale Advances*, 2363-2666.

Muñoz-Echeverri, L., Campo-Avendaño, D., Hoyos-García, M., Velázquez, M. O., Muñoz-Vergara, J., & Giraldo-Correa, G. (2021). Síntesis verde de nanopartículas de ZnO con actividad antibacteriana para funcionalizar textiles de algodón. *Informador Técnico, 85*(2). https://doi.org/10.23850/22565035.3645

Pittayathorn Sratongkham, Rattana Chuenchom, Adisorn Tuantranont, Tanom Lomas, Kamol Wasapinyokul. Non-monotonic evolution of the responses of ZnO-nanoparticle UV-sensitive devices under ambient aging. *Materials Today Communications 2023*, 36 , 106925. https://doi.org/10.1016/j.mtcomm.2023.106925

Sansenya, T., Masri, N., Chankhanittha, T., Senasu, T., Piriyanon, J., Mukdasai, S., & Nanan, S. (2021). Hydrothermal synthesis of ZnO photocatalyst for detoxification of anionic azo dyes and antibiotic. *Journal Of Physics And Chemistry Of Solids, 160*, 110353. https://doi.org/10.1016/j.jpcs.2021.110353

Sarkar, T. (2023). *Estudios estructurales, espectroscópicos y morfológicos sobre nanopartículas verdes de ZnO sint*. https://www.cn.aminer.org/pub/64a390c4d68f896efa1f5208

Shaoqing, Q. (2023). This is a repository copy of Controlling simonkolleite crystallisation via metallic Zn oxidation in a betaine hydrochloride solution.

Sofianos, V. M. (2021). Diverse morphologies of zinc oxide nanoparticles and their electrocatalytic performance in hydrogen production.

Soto, K. G. (mayo de 2023). *Síntesis y caracterización de nanomateriales de ZnO y ZnSe para la producción fotocatalítica de hidrógeno*. Universidad de Ciencias y Artes de Chiapas. https://repositorio.unicach.mx/handle/20.500.12753/4780

Sratongkham, P., Chuenchom, R., Tuantranont, A., Lomas, T., & Wasapinyokul, K. (2023). Non-monotonic evolution of the responses of ZnO-nanoparticle UV-sensitive devices under ambient aging. *Materials Today Communications, 36*, 106925. https://doi.org/10.1016/j.mtcomm.2023.106925

Qu, S., Hadjittofis, E., Malaret, F., Hallett, J., Smith, R., & Campbell, K. S. (2023). Controlling simonkolleite crystallisation via metallic Zn oxidation in a betaine hydrochloride solution. *Nanoscale advances, 5*(9), 2437–2452. https://doi.org/10.1039/d3na00108c

Widiyandari, H., Pratama, E. D., Parasdila, H., Suryana, R., Arutanti, O., & Astuti, Y. (2023). Synthesis of ZnO-Cdots nanoflower by hydrothermal method for antibacterial agent and dye photodegradation catalyst. *Results In Materials, 20*, 100491. https://doi.org/10.1016/j.rinma.2023.100491

Wu, Z., Chen, X., Liu, X., Yang, X., & Yang, Y. (2019). A Ternary Magnetic Recyclable ZnO/Fe3O4/g-C3N4 Composite Photocatalyst for Efficient Photodegradation of Monoazo Dye. *Nanoscale research letters, 14*(1), 147. https://doi.org/10.1186/s11671-019-2974-2

Yabalak, E. (2024). Synthesis of ZnO nanoparticles on the Zn plates recovered from waste batteries using eco-friendly methods and evaluation of its photo-catalytical activity.